



저작자표시-비영리-변경금지 2.0 대한민국

이용자는 아래의 조건을 따르는 경우에 한하여 자유롭게

- 이 저작물을 복제, 배포, 전송, 전시, 공연 및 방송할 수 있습니다.

다음과 같은 조건을 따라야 합니다:



저작자표시. 귀하는 원저작자를 표시하여야 합니다.



비영리. 귀하는 이 저작물을 영리 목적으로 이용할 수 없습니다.



변경금지. 귀하는 이 저작물을 개작, 변형 또는 가공할 수 없습니다.

- 귀하는, 이 저작물의 재이용이나 배포의 경우, 이 저작물에 적용된 이용허락조건을 명확하게 나타내어야 합니다.
- 저작권자로부터 별도의 허가를 받으면 이러한 조건들은 적용되지 않습니다.

저작권법에 따른 이용자의 권리는 위의 내용에 의하여 영향을 받지 않습니다.

이것은 [이용허락규약\(Legal Code\)](#)을 이해하기 쉽게 요약한 것입니다.

[Disclaimer](#)

Master thesis

**Assessment of Adhesion Characteristics of Thermal
Barrier Coatings Using Scratch Test**

The Graduation School of the University of Ulsan

School of Mechanical Engineering

Nguyen Quang Phuong

Assessment of Adhesion Characteristics of Thermal Barrier Coatings Using Scratch Test

Supervisor: Professor Koo-Huyn Chung

A Master Thesis

By

Nguyen Quang Phuong

School of Mechanical Engineering

Ulsan, Korea

Assessment of Adhesion Characteristics of Thermal Barrier Coating Using Scratch Test

This certifies that the dissertation
of Quang-Phuong Nguyen is approved.


Committee Chairman


Professor Kyung-Sick Lee

Committee Member


Professor Sung-Tae Hong

Committee Member


Professor Koo-Hyun Chung

Department of Mechanical Engineering

Ulsan, Korea

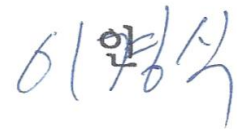
June, 2018

Quang-Phuong Nguyen의

공학석사 학위 논문을 인준함

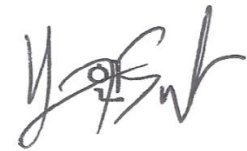
심사위원장

이경식



심사위원

홍성태



심사위원

정구현



울산대학교 대학원

기계자동차공학과

2018 년 6 월

ACKNOWLEDGEMENTS

Firstly, I would like to express my gratitude to my advisor, Professor Koo-Hyun Chung, for support, encouragement, and guidance throughout this research. It is a great understatement to say that this work would not have been possible without my Professor help. Without his kind-hearted support, I would never have the present results.

I would like to thank all members of my laboratory (Tribology Research Laboratory) in a rich environment and collaboration. Their exceptional friendship has made graduate studies more enjoyable.

And I am deeply grateful to the influences and support of professors, colleagues, friends, which is my giant motivation in this thesis journey.

Finally, I would like to share a great deal of my achievement with my parents, my family, and my friends, who always support and encourage me in my life.

ABSTRACT

Assessment of Adhesion Characteristics of Thermal Barrier Coatings Using Scratch Test

Nguyen Quang Phuong

School of Mechanical Engineering

The Graduate School

University of Ulsan

Thermal barrier coatings (TBCs) are advanced materials usually applied to a variety of applications involving high temperature and oxidation such as gas turbines. It is commonly used as protective coatings to improve performance, protect metallic components at elevated temperature and allow higher operating temperatures beyond the limiting temperature of structural components. TBCs structure consists of four layers such as ceramic topcoat, usually 8wt% of YSZ; thin layer of thermally grown oxide (TGO) formed during the service; the metallic bond coat, usually MCrAlY and the metal substrate, usually Ni-based superalloy. The adhesion between the top coat/bond coat interface is an important property in TBCs system. The TGO formed during the service between the top coat/bond coat interface is a necessary layer of a TBC system, providing an oxidation barrier for the underlying component. Unfortunately, TGO is also the main

driver of failure in TBC systems, which affects the adhesion of top coat/bond coat. However, the adhesion characteristic of TBCs are not well understood.

In this work, new approaches to better understand the adhesion of TBCs by using the scratch test based on the Burnett and Rickerby model was used. The relationship between the adhesion of the top coat/bond coat and TGO formed during service was investigated. The cycle thermal fatigue test was used to reproduce the working condition of the TBCs system in the hot section. TBCs were also investigated the lifetime and failure characteristics after the thermal cycle fatigue test. The outcomes of this work may provide a useful guideline for work of adhesion characteristic of TBCs using the scratch test. In addition, the results of this work were expected to be useful to gain an in-depth understanding of the most probable combination and identifying a relationship of the work of adhesion with the thermal cycle fatigue test to use in a life prediction model.

CONTENTS

1. Introduction	1
1.1 Review of Thermal Barrier Coatings	1
1.2 Organization	3
2. Background.....	4
2.1 Thermal Barrier Coating System	4
2.2 Yttria Stabilized Zirconia - Top Coat	5
2.3 Intermetallic Bond Coat	7
2.4 Thermally Grown Oxide	8
3. Experimental Procedure	8
3.1 Specimen Preparation of TBCs.....	8
3.1.1 Sectioning and Mounting.....	9
3.1.2 Grinding and Polishing	10
3.2 Thermal Fatigue Testing	10
3.3 Scratch Adhesion Testing	11
3.3.1 Adhesion Definition.....	12
3.3.2 Adhesion measurement.....	13
3.3.3 Burnett and Rickerby Model	15
3.4 Characterization Method.....	16
3.4.1 Confocal Microscopy.....	16

3.4.2 Micro Vickers Hardness	17
3.4.4 Energy Dispersive X-ray Spectroscopy (EDS)	18
4. Results and Discussion	19
4.1 Microstructure of TBCs	19
4.2 Thermally Grown Oxide	20
4.3 Mechanical Properties and Statistical Analysis of TBCs	23
4.3.1 Porosity of TBCs	23
4.3.2 Hardness of TBCs.....	24
4.3.3 Elastic Modulus	25
4.4 Adhesion Measurement of TBCs.....	26
4.4.1 Scratch Test Results of TBCs.....	26
4.4.2 Scratch Test Behavior of TBCs	31
4.4.3 Work of Adhesion of TBCs.....	32
5. Conclusions and Future Work.....	34
REFERENCES	36

LIST OF FIGURES

Fig. 1 Cross-section of gas turbine RM-12 aero engine [courtesy: GKN Aerospace]....	1
Fig. 2 The evolution of allowable gas temperature at the entry to the gas turbine and the contribution of superalloy development, film cooling technology, thermal barrier coatings and (in the future) ceramic matrix composite (CMC) air foils and perhaps novel cooling concepts.[5]	2
Fig. 3 Schematics of four layers thermal barrier coatings system. The temperature of topcoat is much higher than that of substrate.	4
Fig. 4 Schematics of thermal spray deposition process for thermal barrier coatings.....	6
Fig. 5 (a) Cutting machine Allied, (b) grinder/polisher Allied, (c) epoxy set Pale.....	9
Fig. 6 Thermal fatigue tester	11
Fig. 7 Scratch tester	11
Fig. 8 (a) Confocal microscopy VK-X210, (b) Micro Vickers Hardness HM-123	17
Fig. 9 Confocal microscope images of cross-section microstructure of (a) normal TBC, (b) DVC-TBC (dense vertical crack, DVC), (c) EDC-TBC (extra dense vertical crack, EDC) deposited by APS before thermal fatigue test.	19
Fig. 10 High magnification of the evolution of TGO of (a) normal TBC after 350 cycles thermal fatigue test, (b) DVC-TBC after 350 cycles thermal fatigue test, (c) EDC-TBC after 100 cycles thermal fatigue test.	20
Fig. 11 Energy dispersive x-ray spectroscopy recorded from thermally grown oxide.	21
Fig. 12 TGO growth during thermal fatigue test.....	22
Fig. 13 (a) Porosity of TBCs top coat with different cycle TFT, (b) hardness values of TBCs top coats with different cycle TFT.....	24

Fig. 14 Elastic modulus of TBCs top coat.....	26
Fig. 15 Scratch test result of normal TBC specimen after 250 cycles TFT	28
Fig. 16 Scratch test result of DVC-TBC specimen after 250 cycles TFT.....	29
Fig. 17 Scratch test result of EDC-TBC specimen before TFT	30
Fig. 18 Scratch behavior of TBCs specimen	32
Fig. 19 Work of adhesion of TBCs with different cycle TFT	33

LIST OF TABLES

Table 1 Factors affecting the critical load for coating detachment. [17]	14
Table 2 Elements and their weight in the thermally grown oxide.	22

1. Introduction

1.1 Review of Thermal Barrier Coatings

Thermal barrier coatings (TBCs) is a multilayer material, ceramic and metal, which is commonly used as protective coatings for gas turbine to improve performance, protect metal components from the hot gas stream in the high temperature sections of the engine. At present, the ideal power output increases with the gas temperature at the turbine inlet, but as the gas temperature rises, the work required to provide the cooling air flow necessary to bring the hot section material into their temperature limitations.[1] TBCs is proposed to use as a protective layer between the hot gas stream and the component surface, which usually reduces the maximum surface temperature of the component by 200 °C. The lower surface temperature allows the engine designer to reduce the cooling air to raise efficiency, increase power, increase the turbine inlet temperature, and improve component durability.[1] The TBCs coated in the gas turbine can be seen in Fig. 1.

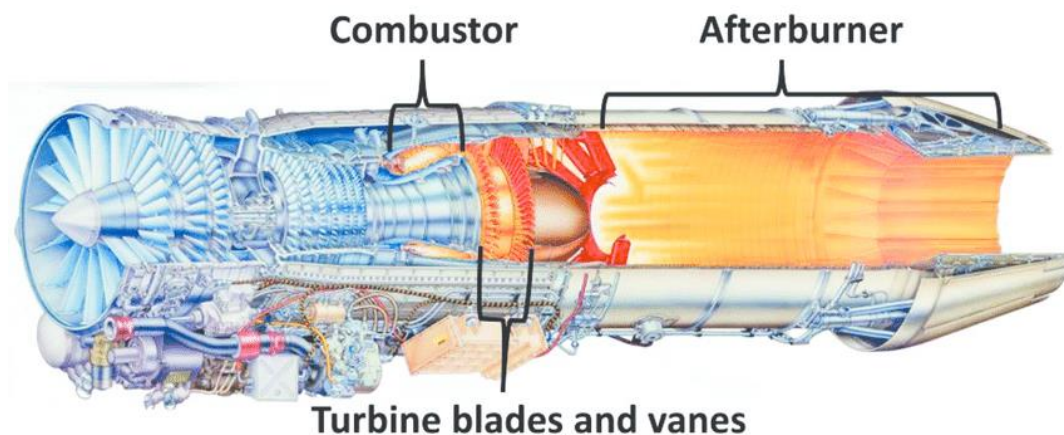


Fig. 1 Cross-section of gas turbine RM-12 aero engine [courtesy: GKN Aerospace]

The evolution of the allowable gas temperature in gas turbine is shown in Fig. 2. The modern thermal barrier coating was introduced in the 1970s, but TBCs were developed as an alternative layer, which were applied to aerospace applications in the 1950s and used in relatively undemanding roles.[2, 3] Air or atmosphere plasma spray developed as branch of research into arc engines, is proven to be an efficient and effective way of depositing TBCs. By 1970s, ceramic coatings were used in hot-sections of aircraft engines.[3] In 1978s, more advanced applications and high temperature of the TBCs were found, which 6-8% YSZ optimized the durability of coatings in typical operation.[4]

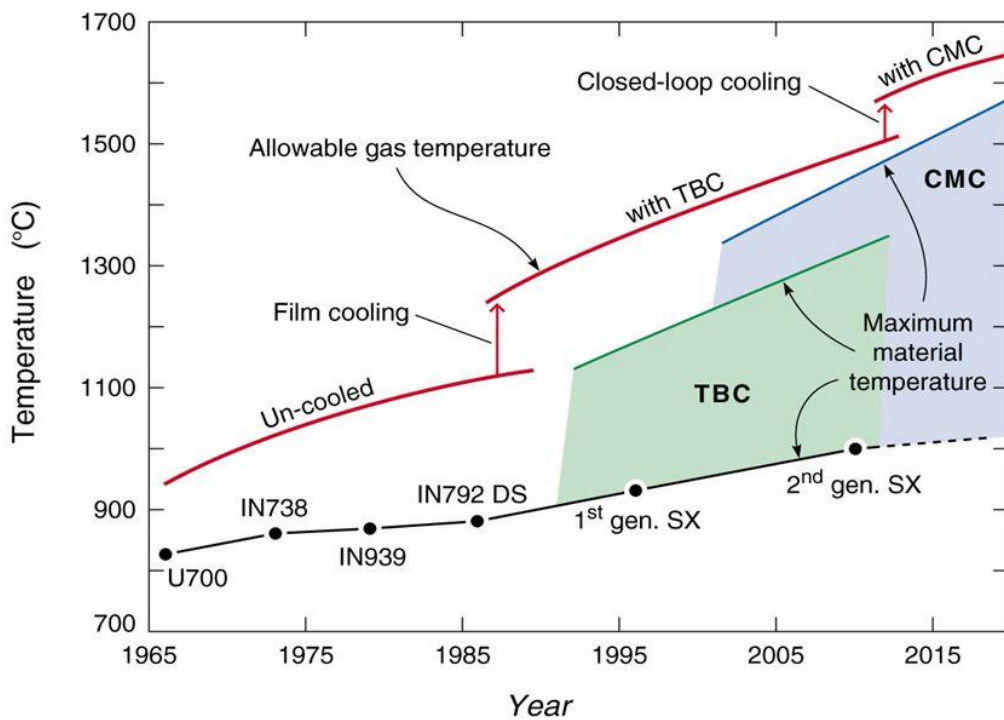


Fig. 2 The evolution of allowable gas temperature at the entry to the gas turbine and the contribution of superalloy development, film cooling technology, thermal barrier coatings and (in the future) ceramic matrix composite (CMC) air foils and perhaps novel cooling concepts.[5]

The temperature of the hot gas in the combustor and at the turbine inlet is typically much hotter than the melting temperature of the superalloy components, which is usually around 1300 °C.[4] In the gas turbine, the cooling and heating cycles of the TBC are frequent and rapidly during many cycles. As in the power generation turbine, cooling and heating cycles are infrequent during service. Due to the anxiety about premature failure, TBCs systems in practice are not designed to their full potential, that although TBCs are over 30 years old, they are still not well understood.[6] The high temperature interplay between mechanical and material phenomena include thermal fatigue, diffusion of oxygen through the top coat, oxidation between the top coat/bond coat interface, sintering during the service leads to complex and sensitive stress states, making life prediction difficult. A reliable, robust, physically-based life prediction model would allow designs that lead to a greater realization of the increases in engine efficiency and performance.

1.2 Organization

This thesis seeks new approaches to understand the work of adhesion of TBCs by: (1) using the scratch test based on Burnett and Rickerby model to figure out the adhesion through careful experimental observations, (2) systematically studying all the mechanical and material phenomenological configurations of three different structure TBCs, (3) developing an in-depth understanding of the most probable combination and identifying a damage parameter that lends itself to use in a life prediction model.

2. Background

2.1 Thermal Barrier Coating System

As shown in Fig. 3 four layers of TBC system: (a) ceramic top coat, typically yttria-stabilized zirconia (YSZ); (b) thin layer of thermally grown oxide (TGO) that forms during service; (c) an intermetallic bond coat, typically MCrAlY or an aluminide; and (d) the substrate, or underlying component is usually a Ni-based superalloy.

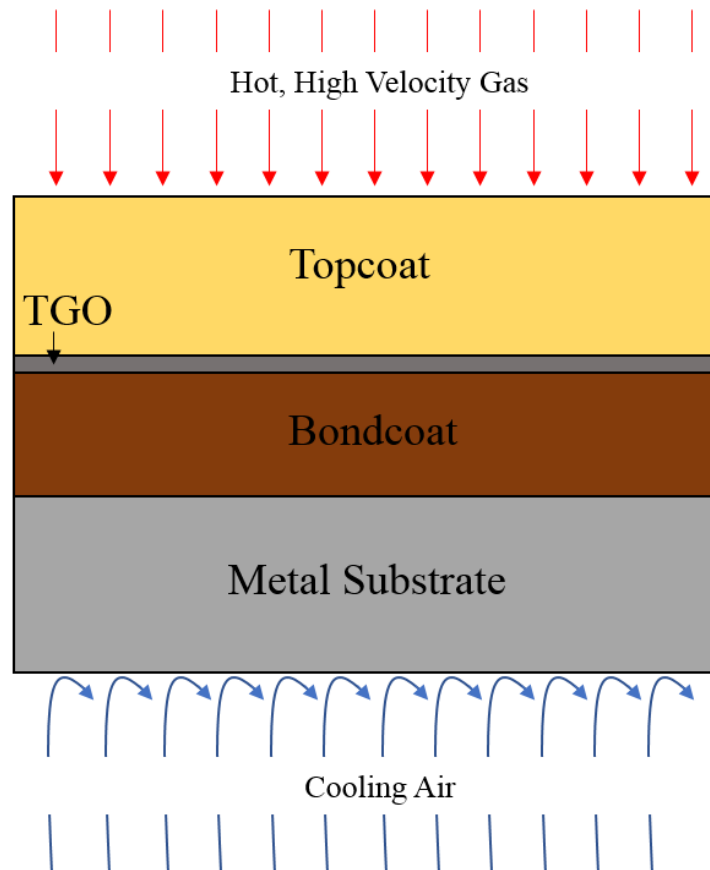


Fig. 3 Schematics of four layers thermal barrier coatings system. The temperature of topcoat is much higher than that of substrate.

2.2 Yttria Stabilized Zirconia - Top Coat

The TBCs top coat is the component which provides thermal insulation properties for the TBCs system. The materials used for the ceramic layer are determined by a number of factors:

- ✓ Materials with low thermal conductivities.
- ✓ A high melting temperature is also required.
- ✓ The thermal expansion coefficient is also very important to allow the ceramic to expand and contract with the component without cracking.
- ✓ Low stiffness are required as well, so that the ceramic can absorb any strain imposed upon it by thermal mismatch.
- ✓ Chemically stable at high temperature.
- ✓ Other desirable material properties include phase stability to avoid large strains due to transformation, a low density to promote strain tolerance and reduce weight, and a high hardness to resist erosion and foreign body impact.

The material that is most widely chosen in the industry is Zirconia, 6-8% yttria partially stabilized zirconia (YSZ) which has a high coefficient of thermal expansion ($\sim 11 \times 10^{-6} \text{ }^\circ\text{C}^{-1}$) [6] and very low thermal conductivity, its around 2.25 W/mK in bulk form and the region of 1 W/mK for a standard TBC coating.[7, 8] It resists corrosion, and it has a sufficiently high melting temperature of about 2700 °C and holds up well to impact with a hardness of around 14 GPa. [6]

In industry, TBCs are produced by many different techniques and a direct outcome is the range of different thicknesses that can be achieved with each of them. The methods used to deposit YSZ top coat include electron beam physical vapor deposition (EBPVD), air or atmosphere plasma spray (APS), high velocity oxygen fuel (HVOF), electrostatic spray-assisted vapor deposition (ESAVD), and direct vapor deposition. These methods are most widely accepted by the industry due to the efficiency, reliability and the resulting microstructures they permit.

In this work, the APS method used to produce the TBCs specimens with laminar structure, and it is providing a reduced elastic modulus and improved deformation resistance of top coat. The APS method with its economic benefits is still preferred commercially, in contrast to the use of the complex and expensive EBPVD. APS method requires a rough bond coat surface for adhesion. Besides, the corrugation of the bond coat surface induces out-of-plane tension in the YSZ during thermal cycling can be harmful to the lifetimes of the coating. This inherent unpredictability is largely what limits APS coatings to non-critical applications.

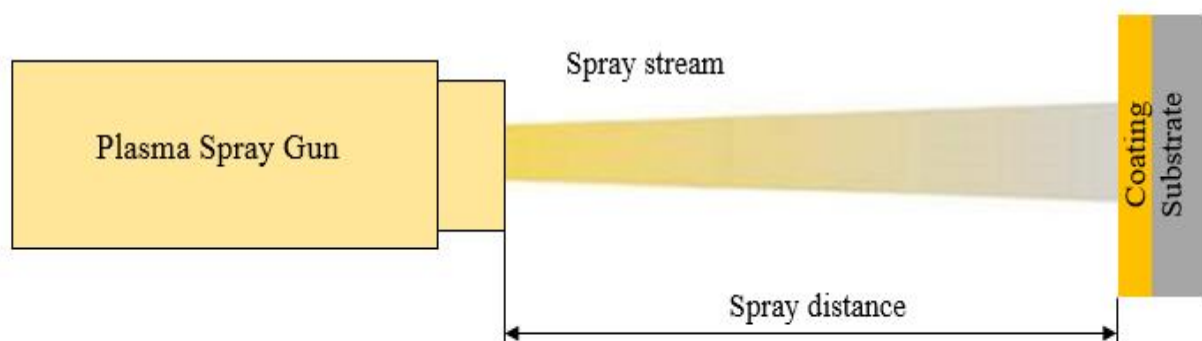


Fig. 4 Schematics of thermal spray deposition process for thermal barrier coatings

As shown in Fig. 4 a schematic of the air plasma spray process used to produce the TBCs specimens. The ceramic top coat deposited by APS method begins as a powder and is injected into a high velocity flame coming from a plasma gun. The plasma gun works by ionizing high velocity carrier gas, usually argon and hydrogen or nitrogen and hydrogen, passing through a DC arc inside the gun, turning it into a plasma. The resulting plasma jet reaches temperatures of up to 6000-12000 °C, [9] melting the YSZ powder and spray it towards a substrate. When the molten YSZ impacts the substrate, it cools, creating a splat. The final coating is a multitude of these splats, creating the characteristic splat boundaries which make up the YSZ top coat microstructure.

2.3 Intermetallic Bond Coat

The bond coat provides a number of functions to the TBCs systems:

- ✓ Protection of the substrate from oxidation and corrosion to prevent the oxygen that passes through the top coat, turning it into Al_2O_3 (TGO).
- ✓ Reduction in the interface stress due to the mismatch in thermal expansion coefficients between top coat and substrate component.
- ✓ Improved adhesion between the top coat and the substrate.

Many techniques such as LPPS, APS, high-frequency pulse detonation, HVOF and EBPVD, have been applied to form the bond coat.[10-12] The bond coat used with EBPVD top coats is usually a platinum-aluminide diffusion coating, applied by pack cementation or chemical vapor deposition (CVD). Pt has long been known to improve EBPVD coating life, and recent evidence shows it promotes Al diffusion towards and

Ni diffusion away from the bond coat surface, giving increased preference to the growth of stable Al_2O_3 . [13] Bond coats used with APS top coats are generally MCrAlY coatings (Metal-Chromium-Aluminum-Yttrium, with M is usually Ni, Co, Fe or a combination), produced by APS or low-pressure plasma spray (LPPS). The APS bond coat is widely used in a TBC system because of its economic benefits. A dense bond coat without oxide formation during spraying can be deposited by LPPS or VPS. Therefore, the bond coat prepared by LPPS or VPS has been employed in the most advanced TBCs, [14-16] although their wide application is limited because of their high costs.

2.4 Thermally Grown Oxide

The TGO is a necessary layer of a TBC system, providing an oxidation barrier for the underlying component. Unfortunately, TGO is also the main driver of failure in TBC systems. Oxygen moves through the YSZ top coat, either through connected porosity or directly through the YSZ and reacts with outwardly diffusing aluminum to create a thin layer of Al_2O_3 when it reaches the top coat/bond coat interface.

3. Experimental Procedure

3.1 Specimen Preparation of TBCs

This section describes the techniques used to cut, mount, grind, and polish the TBCs specimens. All the techniques described in this section are standard metallographies preparation techniques.

3.1.1 Sectioning and Mounting

A section of TBCs prepared for next experiment was cut and mounted. The TBCs specimen required low vibration during cutting to avoid damage that may cause spread beyond the polished depth and affect the analysis results. Cutting of specimens were carried out on TECHCUT 5TM ALLIED low-speed wet saw precision cutting machine, using an Allied wafering blade, Fig. 5 (a). The blade was made to rotate into the coating to avoid applying excessive outward force directly to the coating, which could cause the top coat to crack or separate.

The cut sections of TBCs specimens were then mounted in PACE, Tech. Epoxy Set, which consisted of a mixture of 5:1, resin to hardener, Fig. 5 (c). The epoxy effectively binds the specimen together, so no damage can be done during grinding and polishing. Also, during subsequent examination, the presence of an epoxy filled crack gives good evidence that the damaged region was not caused by grinding or polishing.



Fig. 5 (a) Cutting machine Allied, (b) grinder/polisher Allied, (c) epoxy set Pale

3.1.2 Grinding and Polishing

After curing, the mounted of TBCs specimens were ground and polished on either a DUALPREP 3TM GRINDER/POLISHER ALLIED, Fig. 5 (b). Disposable grinding disks were used in 180, 400, 600, 800, 1200, 2000 progression of grit sizes in order to remove a progressively finer amount of material from the specimen. The grinding process consist of several stages, using a higher number of grit sizes for each subsequent stage and the water was used to coolant throughout the grinding stage. Each stage was eliminated the scratches from the previous coarser paper by orienting the specimen perpendicular to previous scratches and noting that these previously oriented scratches are erased. Polishing of the specimens were done with Allied grit polishing suspension with the progression of grit size was 6 μm , 3 μm and 1 μm . The specimens were rinsed with water between stages to remove the transfer of any residual grit from coarser grit present on the specimen surface.

3.2 Thermal Fatigue Testing

The thermal fatigue test used in this work to reproduce the working condition of the TBCs system in hot section is shown in Fig. 6. The thermal fatigue test (TFT) was performed till 100, 150, 200, 240, 250, 300, 350 cycles in the furnace with a temperature was about 1100 °C. The TBCs specimens were removed at different cycle TFT of their life for cross-sectional studies, while others were observed to 350 cycles. The TFT had the control system consists of temperature control system, a transfer system with transfer arms on both side and five specimens can be held on each side. The transfer system used the compressed air system control. The furnace was kept stable at 1100 °C. After 25

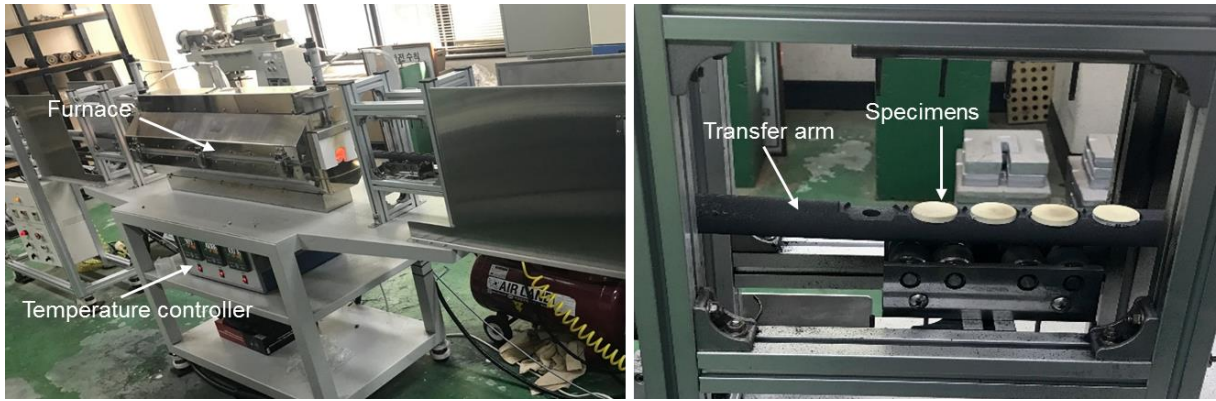


Fig. 6 Thermal fatigue tester

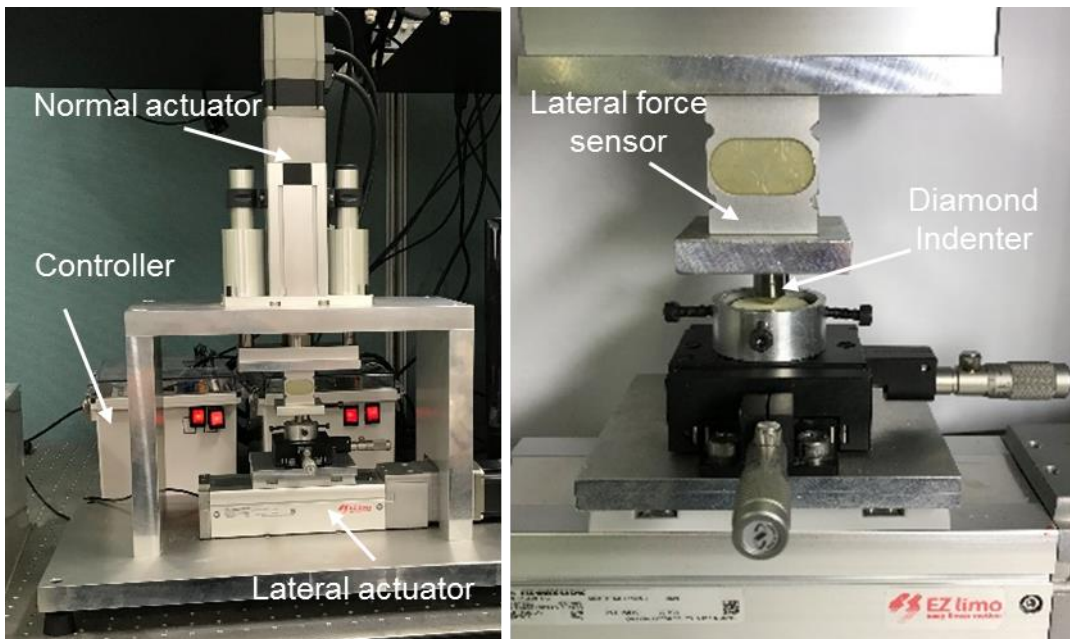


Fig. 7 Scratch tester

minutes heating, the two arms were pulled out to cool the specimens outside the air in 5 minutes. Then the transfer arm was pushed the specimen into the furnace and repeats the cycle.

3.3 Scratch Adhesion Testing

As Fig. 7 showed the photographs of the experimental setup of scratch tester used in this work. This tester has a Rockwell C diamond stylus in the form of a 120° cone

with a spherical tip of radius 200 μm . The diamond indenter moves over a coated substrate under a load which increases from 12.5 to 100 N together with the scratch table speed were kept constant at 4 mm/min. As the diamond indenter scratches the coated substrate, the lateral force signal generated due to cracking or detachment of the coating was picked up by a lateral force sensor. More than five identical scratches were produced on each specimen following the above test parameters.

In addition, the thickness of top coat of TBCs specimens used in this experiment was carefully reduced to less than 50 μm by grinding and polishing process. According to S. J. Bull et al, the scratch test cannot measure the adhesion of a coating greater than 50 μm thick since it cannot generate enough pressure at the interface before the chipping of the coating occurs.

3.3.1 Adhesion Definition

According to the ASTM definition (D907-70),[17] adhesion is the state in which two surfaces are held together by interfacial forces. These bonding forces can be van der Waals forces, electrostatic forces or chemical bonds across the coating-substrate interface. A distinction must be made between basic adhesion which is the highest possible achievable adhesion value, and experimental adhesion that depends on the test type method, the levels of residual stress in the film, or the interfacial flaw distribution.

Experimentally adhesion can be measured in two ways, considering either forces or energy. In terms of forces, the force of adhesion is defined as the minimum force per unit area required to separate the coating from its substrate. In terms of energy, the work

of adhesion, W_{AD} , is defined as the work done in separating the coating from the substrate and is given by Eq. (1):

$$W_{AD} = \gamma_1 + \gamma_2 + \gamma_{12} \quad (1)$$

where γ_1 and γ_2 are the specific surface free energies of components 1 and 2 and γ_{12} is the specific interfacial free energy.[17] In cases where plastic deformation takes place in the interfacial region on coating detachment, an extra term γ_p must be added which often dominates the behaviour.

3.3.2 Adhesion measurement

There are several tests used to characterize the practical adhesion of the coating.[18] Axial tensile forces, bending moments and shear forces can all play a role and the adhesion component is difficult to isolate from the test. If epoxy resins are required to bond the test pieces together, the test is then limited to the tensile strength of the adhesive, which can vary depending on the preparation.[19] Hence the test results are difficult to compare between sets and even within a given set.[19] Of the tests listed below (Table 1), the mechanical methods are of most practical interest. The indentation and scratch tests are the two methods which provide the most useful and repeatable data.

An ideal test for measuring practical adhesion should be: [17]

- ✓ Non-destructive (the commonly used tests are destructive in nature);
- ✓ Easily adapted to routine testing of geometrically complex shapes;
- ✓ Relatively simple to perform and interpret;
- ✓ Amenable to standardization and automation;

- ✓ Reproducible and if possible quantitative;
- ✓ Directly related to coating reliability in specific applications.

Table 1 Factors affecting the critical load for coating detachment. [17]

Qualitative	Quantitative
Mechanical methods	
Scotch tape chest Abrasion test Bend and scratch test	Direct pull-off method Laser Spallation test Ultracentrifuge test Indentation test Substrate training test Scratch test
Non-mechanical methods	
X-ray diffraction	Thermal method Nucleation test Capacity test

In this work, scratch test was used to characterize adhesion of TBCs. The test consists of applying a continuously increasing load on the coating surface by a Vickers or a Rockwell C scratching point while the specimen is displaced at constant speed. The scratch test causes an increasing parallel crack in the scratch track as the load increases. In practice, the coating is seldom removed entirely from the channel, so it is convenient to define a critical load, L_C , which characterizes the mechanical adhesive strength of the coating/substrate system. The lower critical load is taken as the load at which the coating shows the first signs of failure while the upper critical load corresponds to the point where the coating is removed in a regular way along the whole channel length. However,

since there is a defect in the top coat/bond coat interface, isolated areas of coating removal occur, and the critical transitions can be somewhat subjective.[20]

Different techniques for the determination of the critical load of coated products have been implemented.[20]

- Reflected light or confocal microscopy: microscopic observation allows the determination of the critical load and the adhesion quality by examination of the nature of the failure mode and of the extent of the damage;
- Residual depth during the scratch track which can be determined in the cross-sectional profile of the scratch track.
- Change of the friction coefficient: in cases where the adhesion between the coating and substrate and between the coating and stylus are quite different, there is a change in friction coefficient when the substrate is uncovered;

3.3.3 Burnett and Rickerby Model

In this work, adhesion characteristics of TBCs were measured by using scratch test which is the same manner as in the thin and hard coatings. A qualitative measure of the work of adhesion of a top coat/bond coat of TBCs can generally be achieved using the scratch test. The diamond indenter is drawn across the top coat surface under increasing load until some failure occurs at a load which is called the critical load L_c .

A model has been used for the test which relates the measured critical force to the work of adhesion was developed by Burnett and Rickerby's. according to. [21, 22] This model was based on the assumption that the coating was separated from the substrate to

minimize elastic energy. The relationship between the critical force and the work of adhesion can be obtained from the Eq. (2)

$$L_C = \frac{\pi d^2}{8} \left(\frac{2EW}{t} \right)^{1/2} \quad (2)$$

where W is work of adhesion, t is thickness, E is elastic modulus, d is the scratch channel width, L_C is the critical load for interfacial failure.

Hence, a plot of L_C as a function of d^2/t^2 gives a straight line of slope $(2EW)^{1/2}\pi/8$ from which W can be calculated. The work of adhesion can be calculated for a coating of known thickness, elastic modulus, track width and the critical load. It is important to note that it has been assumed in the model that all the stored energy is released once interfacial failure occurs. However, this may not always be the case and thus the work of adhesion is likely considerably smaller.

3.4 Characterization Method

3.4.1 Confocal Microscopy

Polished cross section specimens as well as some failure surfaces were examined by confocal microscope. The confocal microscope used was a VK-X210 KEYENCE, Fig. 8 (a). By means of confocal laser scanning microscopy, it is possible to determine three-dimensional color pictures of surfaces with a high resolution and focus depth. The procedure is nondestructive since the surface is only irradiated by laser emission. The

existing system at the IOT for this surface analysis method is a VK-X210 made by Keyence GmbH, Neu-Isenburg, Germany. The microscope is equipped with an additional xy-axis positioning table that can observe large-area images by combining images. Most of the failure characterization and all of the TGO measurements were performed on this microscope.

3.4.2 Micro Vickers Hardness

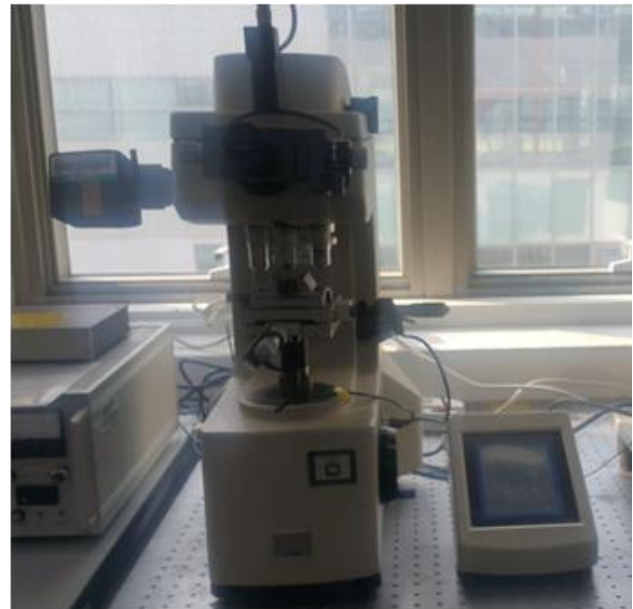
The micro indentation machine used was a Micro Vickers Hardness HM-123, Mitutoyo, Fig. 8 (b). Microhardness is a test performed at low loads, mostly below 1 kilogram-force (kgf). Indentation for specimens were conducted on the sectional plane at 0.3 (kgf), result observation using the built-in measurement tool.

(a)



(Keyence . Inc)

(b)



(Mitutoyo . Inc)

Fig. 8 (a) Confocal microscopy VK-X210, (b) Micro Vickers Hardness HM-123

The test is based on measurement of deformation in the surface caused by the specific shape of indenter impressed with a known force. The Vickers test uses a square-based diamond pyramid indenter with an apical angle of 136° . [23]. The hardness unit of the Vickers test is HV number, which is determined as the ratio F/A , where F is applied force to the indenter in kgf and A is the area of the indentation in mm^2 .

3.4.4 Energy Dispersive X-ray Spectroscopy (EDS)

Energy Dispersive X-ray Spectroscopy (EDS) technique has been used in this work to obtain the composition of TGO formed between the top/bond coat after TFT. EDS mapping of the TGO provides the qualitative information about the different elements present in the TGO.

On the fact, the ability of EDS to detect element based on each element has a unique atomic structure due to that the emission of X-rays is exclusive to a particular element. The vacancies appeared during the process that the electron beam interact with the specimen and knocked out some electrons in the specimen's elements which were filled by electrons after that from other shells resulting in the emission of characteristic X-rays. These X-rays are then detected by the EDS detector.

4. Results and Discussion

4.1 Microstructure of TBCs

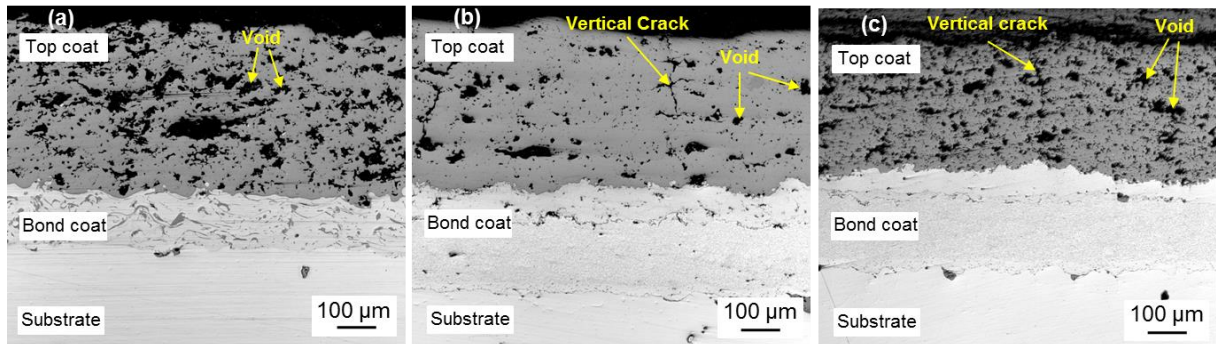


Fig. 9 Confocal microscope images of cross-section microstructure of (a) normal TBC, (b) DVC-TBC (dense vertical crack, DVC), (c) EDC-TBC (extra dense vertical crack, EDC) deposited by APS before thermal fatigue test.

As shown in Fig. 9 confocal microscope images of three different types of TBCs (a) normal TBC, (b) DVC-TBC, (c) EDC-TBC. In Fig. 9 (a), the cross-sectional microstructures of normal TBC showed high porosity, where the black areas are porous and grey areas are solid ceramic, in the top coat. While the cross-sectional microstructures of DVC-TBC top coat showed defects, such as the dense vertical crack (DVC) and porosity as shown in Fig. 9 (b). In the case of EDC-TBC, the cross-sectional microstructures of top coat showed high porosity and dense vertical crack, Fig. 9 (c). The vertical cracks of DVC-TBC and EDC-TBC formed during the spray coating with high temperature and high velocity plasma jet. Taylor [24] invented a DVC which has a segmentation crack density network, which improves the deformation tolerance of the coating and thermal resistance of TBCs. The normal TBC topcoat prepared by APS process with normal velocity plasma spray (NVPS), designed for stationary parts. The

DVC-TBC and EDC-TBC top coats prepared by APS process with high velocity plasma spray (HVPS), designed for rotating parts. The top coats prepared by the APS process showed intrinsic defects, such as pores, unmelted particles, and splat boundaries. In the APS process, many small particles are accelerated by the high-power plasma to impinge on the bond coat to form the top coat. The bond coats prepared by the LPPS exhibited similar microstructure with a dense microstructure and no oxide formation, whereas the APS bond coat featured high levels of visible oxides.

4.2 Thermally Grown Oxide

The thermally grown oxide (TGO) thickness measurements were taken with different cycle TFT and were made on the confocal microscope using the built-in measurement tool. Measurements were made locally within several large spaced locations across the interface, in order to account for large scale spatial variations in thickness. Within each location, an average of 15 local measurements was made. The average thicknesses at all the locations across the section were again averaged to obtain

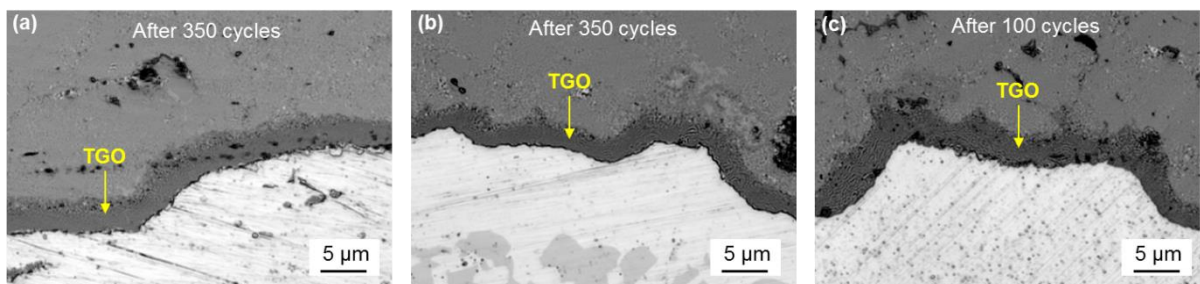


Fig. 10 High magnification of the evolution of TGO of (a) normal TBC after 350 cycles thermal fatigue test, (b) DVC-TBC after 350 cycles thermal fatigue test, (c) EDC-TBC after 100 cycles thermal fatigue test.

the final TGO thickness for the section. As shown in Fig. 10 (a), (b) and (c) high magnification of the evolution of TGO were observed for normal TBC, DVC-TBC and EDC-TBC, the dark gray line (TGO) formed during the thermal fatigue test appears in the interface of top coat/bond coat. The normal TBC showed the thicknesses of TGO are about $3.9 \pm 0.5 \mu\text{m}$ for the specimen after 350 cycles thermal fatigue test, Fig. 10 (a). The DVC-TBC showed the thicknesses of TGO are about $2.9 \pm 0.4 \mu\text{m}$ for the specimen after 350 cycles thermal fatigue test Fig. 10 (b). In the case of EDC-TBC the thicknesses of TGO are about $3.9 \pm 0.3 \mu\text{m}$ for the specimen after 100 cycles thermal fatigue test Fig. 10 (c). The EDC-TBC with the LPPS bond coat was delaminated after 100 cycles, but no delamination was observed in other TBCs.

The TGO was examined by energy dispersive X-ray spectroscopy as shown in Fig. 11. The EDS result of the TGO revealed high concentrations of Al, O, Cr, and

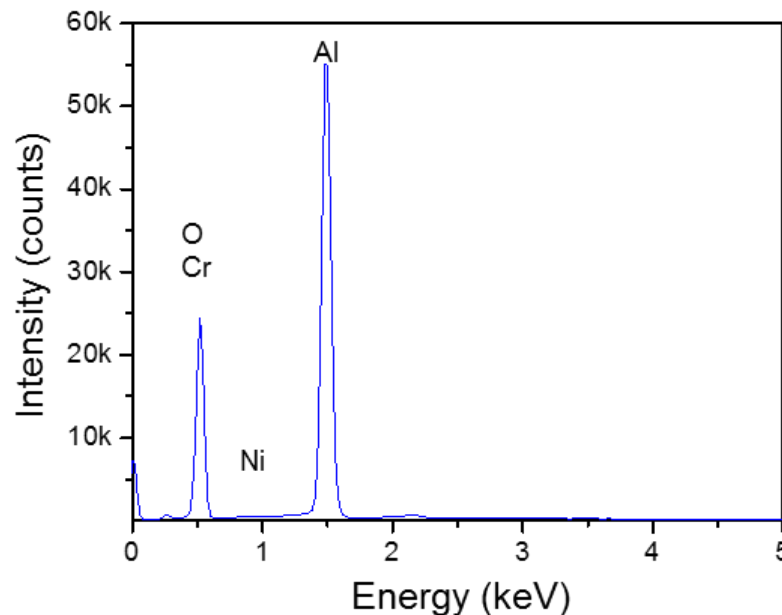


Fig. 11 Energy dispersive x-ray spectroscopy recorded from thermally grown oxide.

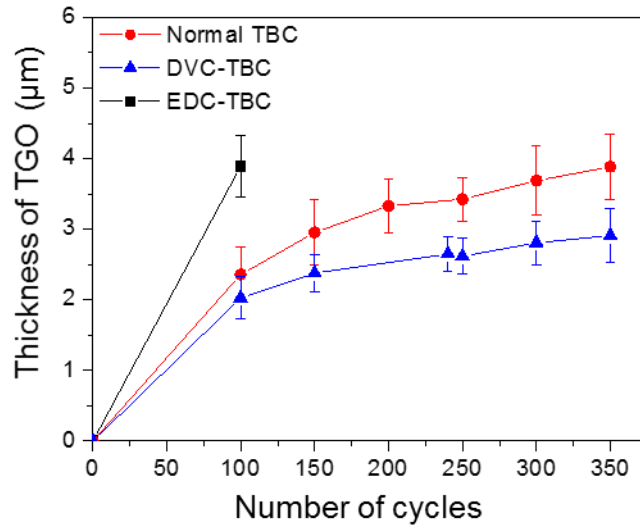


Fig. 12 TGO growth during thermal fatigue test.

Table 2 Elements and their weight in the thermally grown oxide.

Element	Weight%	Atomic%
O K	52.35	65.51
Al K	45.33	33.63
Cr K	1.63	0.63
Ni K	0.69	0.24
Totals	100	

Ni. It can be noted that the main composition was Al_2O_3 in TGO according to the high ratio of Al and Oxy in the EDS results, as showed in table 2.

As show in Fig. 12 during TFT the TGO growth significantly, the average TGO thickness in TBCs increased with the increase of cycle TFT. The normal TBC for different cycles of 100, 150, 200, 250, 300, 350 cycles were measurement yielded the TGO thickness of $2.4 \pm 0.4 \mu\text{m}$, $3 \pm 0.5 \mu\text{m}$, $3.3 \pm 0.4 \mu\text{m}$, $3.4 \pm 0.3 \mu\text{m}$, $3.7 \pm 0.5 \mu\text{m}$, and $3.9 \pm 0.5 \mu\text{m}$. The DVC-TBCs for different cycles of 100, 150, 240, 250, 300, 350 cycles were measurement yielded the TGO thickness of $2 \pm 0.3 \mu\text{m}$, $2.4 \pm 0.3 \mu\text{m}$, $2.6 \pm$

0.2 μm , $2.6 \pm 0.3 \mu\text{m}$, $2.8 \pm 0.3 \mu\text{m}$, and $2.9 \pm 0.4 \mu\text{m}$, respectively. In the case of EDC-TBC the thickness of TGO was $3.9 \pm 0.3 \mu\text{m}$, after 100 cycles thermal fatigue test. In Fig. 3 (b), the thickness of TGO after thermal fatigue test is plotted against the square root of cycles TFT. The result of the TGO growth of normal TBC is greater than that of DVC-TBC. Due to the effect of high porosity of normal TBC leads to a more rapid diffusion of oxygen through the top coat layer, which leads to a faster TGO formation. For DVC-TBC had less porosity which leads to a slower diffusion of oxygen than normal TBC that leads to the slow formation of TGO.

4.3 Mechanical Properties and Statistical Analysis of TBCs

4.3.1 Porosity of TBCs

The porosity was measured using image analysis technique, porosity within a microstructure TBCs top coat was easily detected due to the high degree on contrast between the dark pores and the gray color is the solid ceramic of the top coat. The image analysis result of porosity of the normal TBC, DVC-TBC and EDC-TBC with different cycle thermal fatigue test are shown in Fig. 13 (a), the porosity of normal TBC, DVC-TBC and EDC-TBC were determined before thermal fatigue test to be 29%, 8.6% and 21.2%. After 350 cycles of thermal fatigue test the porosity of normal TBC, and DVC were decreased to 15.9% and 6.3%. In the case of EDC-TBC the porosity was decreased to 17.2% after 100 cycles of thermal fatigue test. The decrease of the porosity is consistent with the microstructural changes observed in the top coat. During the thermal fatigue test, the small pores were sintered, while the larger pores were unaffected. The changes in porosity are consistent with the changes in microstructure at the top coat, which is in good agreement with the microstructural evolution. In addition, the porosity

of normal TBC, DVC-TBC and EDC-TBC were also slightly decreased after reducing the thickness of the top coat. The change of porosity caused by reduced to the reduction of pores and defects due to the reduced thickness of the top coat.

4.3.2 Hardness of TBCs

The changes in the microstructure of the top coat after the TFT some way relation to the change in the hardness value as shown in Fig. 13 (b), The hardness values of the top coat with different cycle TFT were measured using a Vickers indentation method. The indentation tests were conducted on the sectional plane with a load of 3 N at room temperature. The hardness values of the top coats in the normal TBCs were determined to be 288.9 ± 32 HV (mean \pm standard deviation). After the thermal fatigue tests for 100, 150, 200, 250, 300, 350 cycles, the hardness values of the top coats were increased to 310.8 ± 32 , $322. \pm 48$, 360.4 ± 43 , 343 ± 44 , 332.5 ± 29 and 429.4 ± 28 HV.

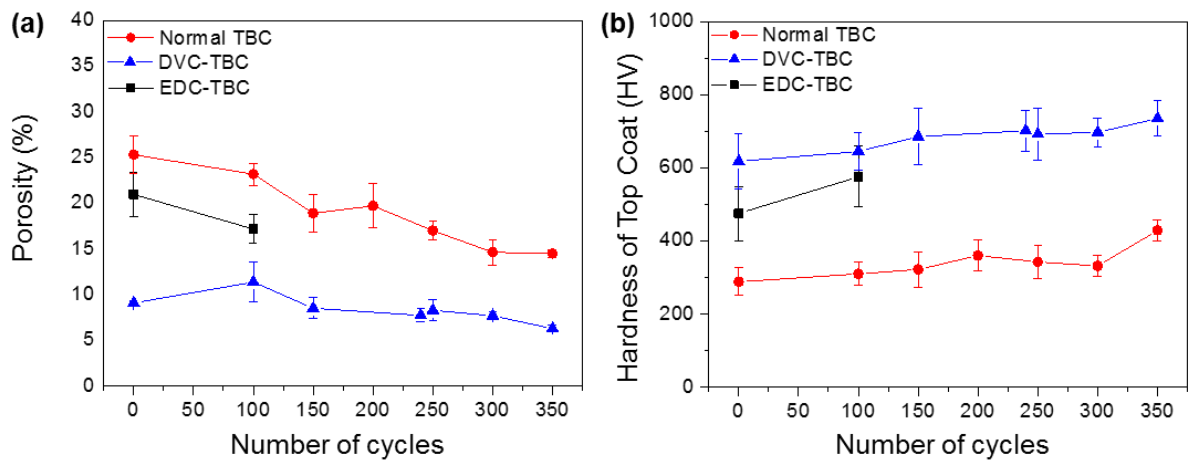


Fig. 13 (a) Porosity of TBCs top coat with different cycle TFT, (b) hardness values of TBCs top coats with different cycle TFT.

The hardness values of the top coats in the DVC-TBCs were determined to be 680.3 ± 83 HV, after the thermal fatigue tests for 100, 150, 240, 250, 300, 350 cycles, the hardness values of the top coats were increased to 709.6 ± 57 , 754.6 ± 84 , 772.4 ± 62 , 761.9 ± 78 , 767.8 ± 43 and 808.8 ± 53 HV, respectively. In the case of EDC-TBCs the hardness values of the top coat were 475.9 ± 74 HV, after 100 cycles fatigue test the hardness was increased to 579.2 ± 76 HV. The EDC-TBC was delaminated after 100 cycles thermal fatigue test. The increase in the hardness values after thermal fatigue test was due to the reduction of pores and defects. In this case, the DVC-TBC, which is less porosity and dense vertical crack, indicates that the hardness value is greater than the normal TBC. Both of normal TBC and DVC-TBC specimens show a slightly increase in hardness value, which is the increase of cycles of thermal fatigue test. The reduction of pores and defects due to the thermal fatigue test in the microstructure of the top coat of normal TBC and DVC-TBC, which increase the density of top coat leading to increased hardness values.

4.3.3 Elastic Modulus

The elastic modulus of the normal TBC and DVC-TBC top coat were analysis based on the Oliver Pharr model. The statistical analysis of the elastic modulus of the coatings are shown in Fig. 14. The nanoindentation was used to characteristic the elastic modulus of normal TBC and DVC-TBC using Berkovich diamond indenter. For the Berkovich indenter the effective half-included angle ϕ is equal to 70.3° . The Poisson's ratio of the diamond tip ν_d is equal to 0.07 and E_d is Young's modulus of diamond equal to 1140 GPa. The Poisson's ratio of the YSZ top coat was taken equal to 0.25. In addition, the elastic modulus of the top coat can be calculated from the Eq. 2. In order

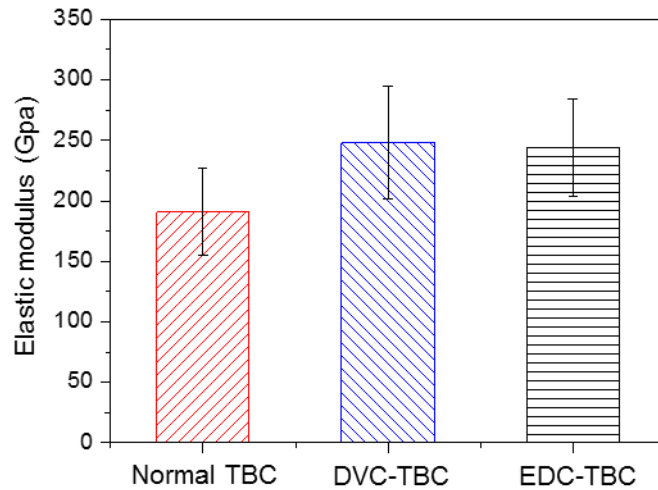


Fig. 14 Elastic modulus of TBCs top coat

to obtain an elastic modulus of normal TBC and DVC-TBC more than ten experiment were make of each specimen. The average of elastic modulus of normal TBC was measured to 191 ± 36 GPa. In the case of DVC-TBC, the elastic modulus is equal to 248 ± 47 GPa. For large-scale reconnaissance measurements, elastic modulus of normal TBC and DVC-TBC were calculated using the built-in measurement tool of the nanoindentation with standard values ϵ is equal to 0.73.

4.4 Adhesion Measurement of TBCs

4.4.1 Scratch Test Results of TBCs

The qualitative analysis of the scratch tracks extended to a quantitative analysis by measuring the critical load values to get an idea about the adhesion of the top coating. By carefully observing the scratch track of the normal TBC, DVC-TBC, and EDC-TBC made under continuous load revealed series of cracks in the ceramic top coating along the scratch track. The critical load is the normal load at which the first sign of coating failure occurs. This critical load was determined by the combination of observations of

scratch track by confocal microscopy, measurements of normal loads, and residual depth during scratch track. In order to evaluate the critical load more than five scratches were made. The average of these loads was taken as the value of the critical load. It has also noticed that as the load increases in a continuous load test, the density of parallel cracks in the scratch track is substantially increased. This result leads to increased stress in the coating and, therefore, an increased crack density. At a few places on the scratch track, it was found that portions of the coating separated from the top coat, and the debris thus created was found on both sides of the scratch track. These cracks are the tensile cracks formed at the rear of the indenter as described by Burnett et al. [25]

As showed in Fig. 15 the confocal image of scratch track, coefficient of friction (COF), normal force and lateral force of normal TBC specimen after 250 cycles thermal fatigue test were calculated and plotted. The relation of coefficient of friction, normal force and lateral fore are given in Fig. 15. The coefficient of friction and lateral force showed an unstable form. This is the result of changes in penetration depth and fracture of the deformed layer during the scratch test. It was also calculated the critical force of the adhesion failure at 55 N of normal load. The critical force was determined by the first sign of adhesion failure on the confocal image and compared with the coefficient of friction observed.

Scratch test result of DVC-TBC specimen after 250 cycles thermal fatigue test are showed as Fig. 16. This figure showed the confocal image of scratch track, coefficient of friction (COF), normal force and lateral force. It can be seen the failure of the coating

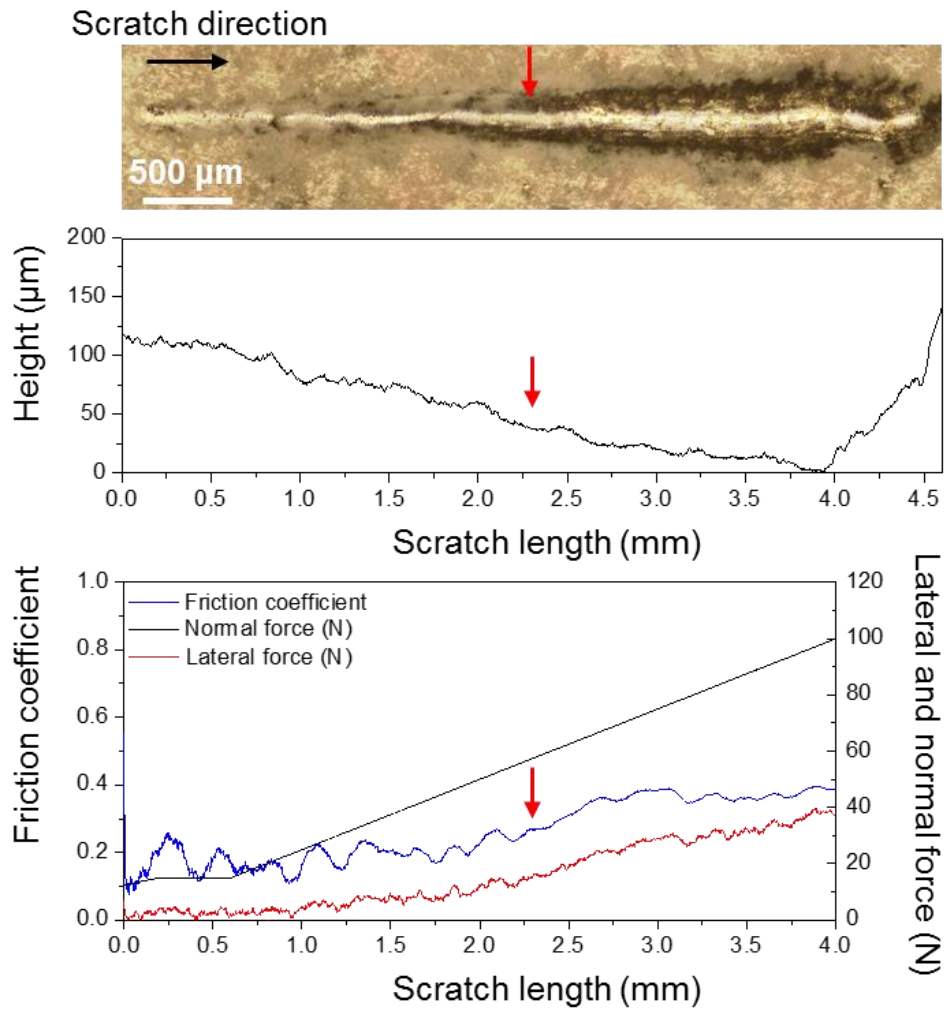


Fig. 15 Scratch test result of normal TBC specimen after 250 cycles TFT

on the scratch line that the critical force of DVC-TBC was indicated by red arrow. It was calculated at 64 N of normal load.

Scratch test result of EDC-TBC before thermal fatigue test are shown as Fig. 17. This figure showed the confocal image of scratch track, coefficient of friction (COF), normal force and lateral force. It can be seen the failure of the coating on the scratch line that the critical force of EDC-TBC was indicated by red arrow. It was calculated at 57 N of normal load.

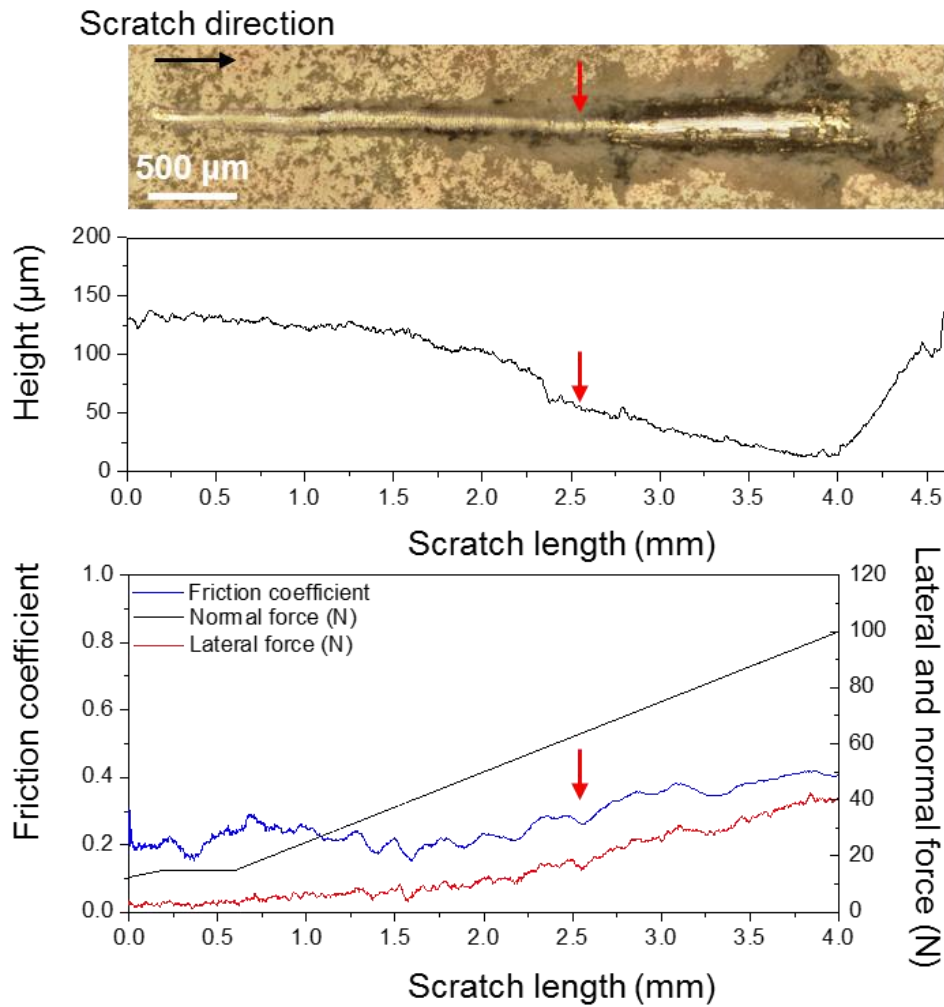


Fig. 16 Scratch test result of DVC-TBC specimen after 250 cycles TFT

In addition, the failure modes on the confocal images of normal TBC, DVC-TBC and EDC-TBC were also observed. During the scratch tracks of normal TBC, DVC-TBC and EDC-TBC, a common failure mode is the spallation in the top coat separates in front of the moving indenter. This failure leads to chipping on the edge of the track, shown in the confocal images of both normal TBC, DVC-TBC, and EDC-TBC. It can be seen the plowing effect in front of the moving indenter due to the increased of load and several coating spallation appear during the test, which is the result of localized chipping to gross spallation.

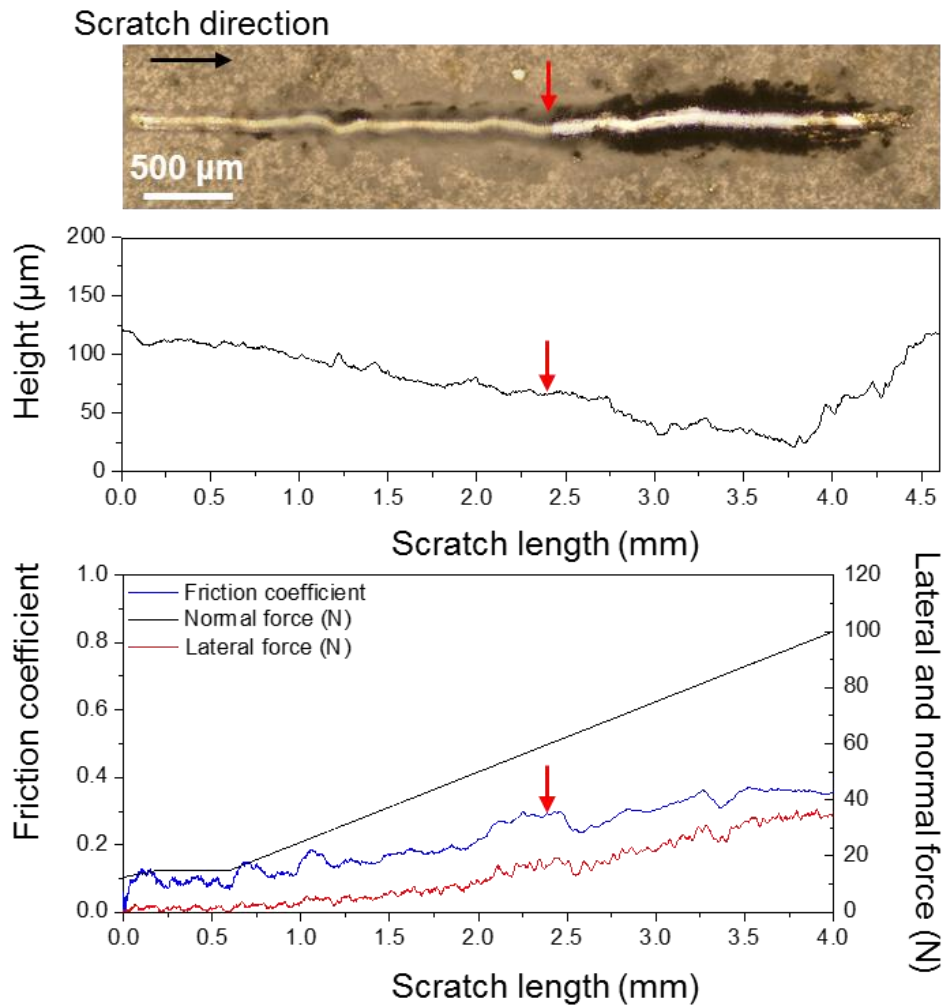


Fig. 17 Scratch test result of EDC-TBC specimen before TFT

It has also noticed that as the load increases in a continuous load test, the density of parallel cracks in the scratch track is substantially increased. This result leads to increased stress in the coating and, therefore, an increased crack density. At a few places on the scratch track, it was found that portions of the coating were separated from the top coat, and the debris thus created was found on both sides of the scratch track. These cracks are the tensile cracks formed at the rear of the indenter as described by Burnett et al.

4.4.2 Scratch Test Behavior of TBCs

A common failure mode is the spallation in which the top coat separates to minimize the amount of elastic energy stored by the large compression stresses in front of the moving indenter. This implies a relatively adhesion and leads to semicircular cracks that propagate outward from the center line of the scratch track. This mode of failure leads to chipping on the side of the track, if the interfacial crack propagates outside the scratch line before the indenter passes over it. This type of failure usually leaves signs of damage in the scratch track and chipping along the edges. As the thickness of the coating increases, this type of failure is more likely. In addition to the chipping on the track, it observed that is not related to any delamination initiated front of the indenter. This is the result of the differential elastic recovery of the coating and the substrate. Such recovery tracks can often be found along with compressive spalling cracks on a given crack segment. The two can be difficult to differentiate. However, as the level of residual stresses in the coating increases, compression spallation failures become more evident. This may also arise from the cracks which form at the rear of the diamond contact in response to the tensile stresses generated during sliding.

During the scratch track, a common failure mode is the spallation in the top coat separates in front of the moving indenter. This failure leads to chipping on the side of the track. With increasing load, a ploughing effect can be seen in front of the moving indenter and several spallation mechanisms appear, from localized chipping to gross spallation, as shown in Fig, 18.

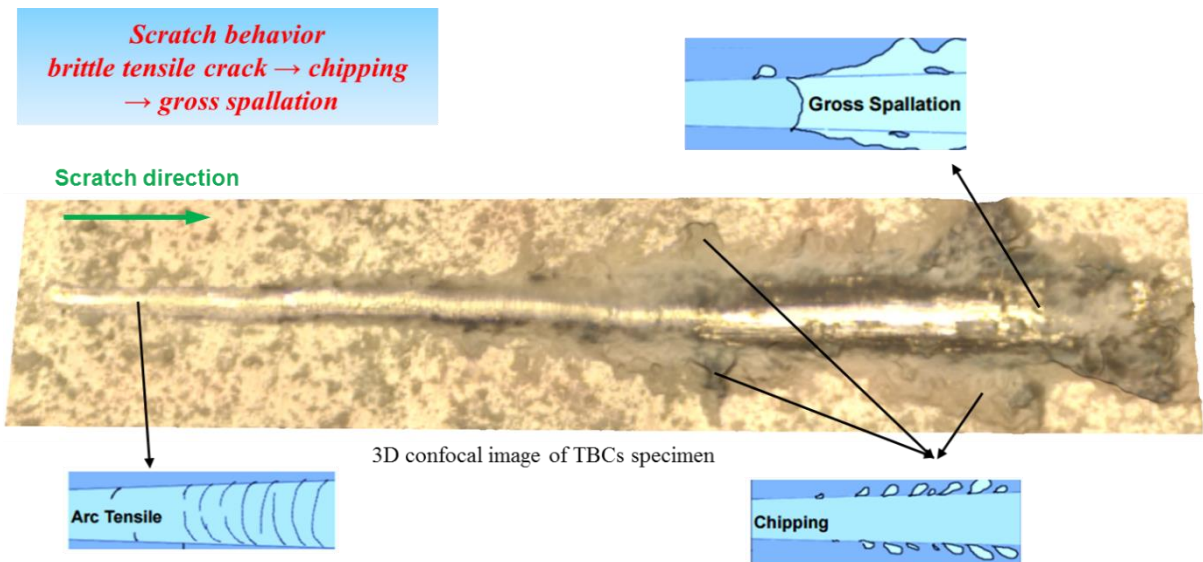


Fig. 18 Scratch behavior of TBCs specimen

4.4.3 Work of Adhesion of TBCs

The change of the work of adhesion of the top coat of normal TBC and DVC-TBC within the thermal cycle fatigue test are given in Fig. 19, where the measurements were based on the scratch adhesion test. The work of adhesion of normal TBCs and DVC-TBC before and after thermal fatigue test is calculated from the experimental data based on Burnett and Rickerby model. It found from this figure was decreased with the increased of cycles thermal fatigue test. The work of adhesion of the normal TBC and DVC-TBC before thermal fatigue test were calculated equal to $118.7 \pm 36.3 \text{ J/m}^2$ and $134.3 \pm 23 \text{ J/m}^2$. After the thermal fatigue test, the work of adhesion of normal TBC and DVC-TBC were also decreased equal to $76.8 \pm 7.3 \text{ J/m}^2$ and $88 \pm 9.4 \text{ J/m}^2$ after 350 cycles thermal fatigue test. In the case of EDC-TBC, the work of adhesion before TFT was calculated equal to $129 \pm 10 \text{ J/m}^2$. From the result, it can be seen the work of adhesion of DVC-TBC was greater than normal TBC. After 100 cycles thermal fatigue

test the work of adhesion of DVC-TBC was decrease from $134.3 \pm 23 \text{ J/m}^2$ to $98.3 \pm 26.5 \text{ J/m}^2$, and slightly decrease to $95.3 \pm 14 \text{ J/m}^2$, $87.7 \pm 11.6 \text{ J/m}^2$, $85.7 \pm 8.6 \text{ J/m}^2$, $86.8 \pm 13.9 \text{ J/m}^2$ and $88 \pm 9.4 \text{ J/m}^2$ after 100, 150, 200, 250, 300 and 350 cycles thermal fatigue test. In the case of normal TBC, the work of adhesion showed an unstable form, but overall the work of adhesion of normal TBC was decreased. The work of adhesion of normal TBC after thermal fatigue tests for 100, 150, 240, 250, 300, and 350 cycles were calculated to $115.5 \pm 29 \text{ J/m}^2$, $89 \pm 7.8 \text{ J/m}^2$, $98.4 \pm 16.6 \text{ J/m}^2$, $83.7 \pm 10.7 \text{ J/m}^2$, $61.4 \pm 13.7 \text{ J/m}^2$ and $76.8 \pm 7.3 \text{ J/m}^2$.

Comparing Fig. 12 with Fig. 19 the formation of TGO was pronounced at the top coat/bond coat interface as indicated by Fig. 3 (a) and (b). Decreasing of the work of adhesion of normal TBC and DVC will effect on the top coat/bond coat, which leads to the failure of the topcoat. It is reasonably interpreted that the decrease in the work of adhesion would be attributed to decrease of top coat strength itself.

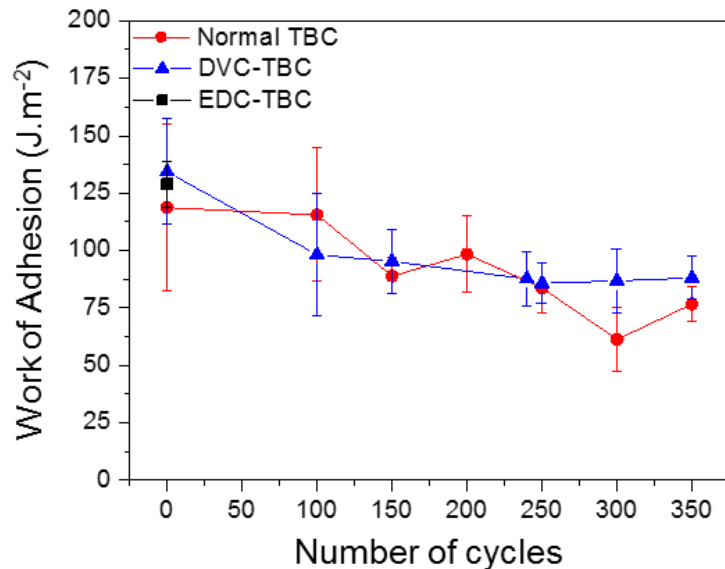


Fig. 19 Work of adhesion of TBCs with different cycle TFT

5. Conclusions and Future Work

This study investigated the scratch adhesion of TBCs. The following conclusions can be drawn:

- ✓ The work of adhesion of normal TBC, DVC-TBC and EDC-TBC were investigated using scratch test. The method described in this study is more accurate and appropriate than methods usually used for thin hard coatings.
- ✓ The adhesion of the TBCs had been found to decrease due to the increase of number of cycles thermal fatigue test.
- ✓ The appearance and increased thickness of TGO during the thermal fatigue test have affected the adhesion between the top coat and bond coat.
- ✓ The effect of high porosity leads to a more rapid diffusion of oxygen through the TBCs top coat, which lead to a faster TGO formation. It will lead to instability of the TBCs top coat.
- ✓ The failure of the EDC-TBC at 100 TFT cycles due to the instability of the top coat with high porosity and vertical cracks.
- ✓ The changes in microstructure of the top coat in some way relate to the change in the hardness values, such as the increase of density during the sintering of small pores.
- ✓ As shown in Fig. 8 the different of work of adhesion of normal TBC, DVC-TBC and EDC-TBC is not clear. Both normal TBC and DVC-TBC are fabricated by APS processes with different temperatures and velocities, which affect the porosity of normal TBC and DVC TBC. Therefore, the work of adhesion of normal TBC and DVC-TBC is not much different. Normal TBC prepared by APS

process with normal velocity plasma shown high porosity and DVC-TBC prepared by APS process with high velocity plasma shown less porosity and vertical crack. Comparison Fig. 12 with Fig. 18 the result of TGO growth of normal TBC is greater than DVC-TBC. The reason for the failure of the adhesion is due to the growth of TGO during the thermal fatigue test that destabilizes the adhesion of the coating. The advantages of DVC-TBC are more evident which higher cycles thermal fatigue test due to the slow formation of TGO of DVC-TBC.

Future work:

- The thermally fatigue test of TBCs could be investigated with higher cycles thermally fatigue test.
- Different thermal barrier coating materials such as lanthanum zirconate ($\text{La}_2\text{Zr}_2\text{O}_7$) could be investigated using the scratch test model.
- The simulation could be carried out to estimate the lifetime of normal TBC and DVC-TBC.

REFERENCES

- [1] J.H. Perepezko, "Materials science. The hotter the engine, the better," *Science*, vol. 326, no. 5956, Nov 20, pp. 1068-1069.
- [2] R.A. Miller, "Thermal barrier coatings for aircraft engines: history and directions," *J. Therm. Spray Technol.*, vol. 6, no. 1, pp. 35.
- [3] R.A. Miller, "History of Thermal Barrier Coatings for Gas Turbine Engines: Emphasizing NASA's Role from 1942 to 1990,".
- [4] S. Stecura, "Effects of compositional changes on the performance of a thermal barrier coating system.[yttria-stabilized zirconia coatings on gas turbine engine blades],".
- [5] R.C. Reed, "The superalloys: fundamentals and applications," 2008.
- [6] N.P. Padture, M. Gell and E.H. Jordan, "Thermal barrier coatings for gas-turbine engine applications," *Science*, vol. 296, no. 5566, Apr 12, pp. 280-284.
- [7] C.G. Levi, "Emerging materials and processes for thermal barrier systems," *Current Opinion in Solid State and Materials Science*, vol. 8, no. 1, pp. 77-91.
- [8] J. Brandon and R. Taylor, "Phase stability of zirconia-based thermal barrier coatings part I. Zirconia-yttria alloys," *Surface and Coatings Technology*, vol. 46, no. 1, pp. 75-90.
- [9] S.M. Meier and D.K. Gupta, "The evolution of thermal barrier coatings in gas turbine engine applications," *Journal of Engineering for Gas Turbines and Power*, vol. 116, no. 1, pp. 250-257.
- [10] Y. Li, C. Li, G. Yang and L. Xing, "Thermal fatigue behavior of thermal barrier coatings with the MCrAlY bond coats by cold spraying and low-pressure plasma spraying," *Surface and Coatings Technology*, vol. 205, no. 7, pp. 2225-2233.
- [11] J. Haynes, M. Ferber, W. Porter and E. Rigney, "Mechanical properties and fracture behavior of interfacial alumina scales on plasma-sprayed thermal barrier coatings," *Materials at High Temperatures*, vol. 16, no. 2, pp. 49-69.
- [12] A. Peichl, T. Beck and O. Vöhringer, "Behaviour of an EB-PVD thermal barrier coating system under thermal-mechanical fatigue loading," *Surface and Coatings technology*, vol. 162, no. 2-3, pp. 113-118.

- [13] K.A. Marino and E.A. Carter, "The effect of platinum on Al diffusion kinetics in β -NiAl: Implications for thermal barrier coating lifetime," *Acta Materialia*, vol. 58, no. 7, pp. 2726-2737.
- [14] B.K. Pant, V. Arya and B. Mann, "Development of low-oxide MCrAlY coatings for gas turbine applications," *J. Therm. Spray Technol.*, vol. 16, no. 2, pp. 275-280.
- [15] K.W. Schlichting, N. Padture, E. Jordan and M. Gell, "Failure modes in plasma-sprayed thermal barrier coatings," *Materials Science and Engineering: A*, vol. 342, no. 1-2, pp. 120-130.
- [16] A. Rabiei and A. Evans, "Failure mechanisms associated with the thermally grown oxide in plasma-sprayed thermal barrier coatings," *Acta materialia*, vol. 48, no. 15, pp. 3963-3976.
- [17] D. Rickerby, "A review of the methods for the measurement of coating-substrate adhesion," *Surface and coatings technology*, vol. 36, no. 1-2, pp. 541-557.
- [18] P. Steinmann and H. Hintermann, "A review of the mechanical tests for assessment of thin-film adhesion," *Journal of Vacuum Science & Technology A: Vacuum, Surfaces, and Films*, vol. 7, no. 3, pp. 2267-2272.
- [19] H.F. Gertsen-Briand, "Characterization of sol-gel yttria stabilized zirconia thin films deposited on metallic substrates."
- [20] D.S. Rickerby and A. Matthews, "Advanced surface coatings: a handbook of surface engineering," 1991.
- [21] P.J. Burnett and D. Rickerby, "The mechanical properties of wear-resistant coatings: I: Modelling of hardness behaviour," *Thin Solid Films*, vol. 148, no. 1, pp. 41-50.
- [22] S. Bull, D. Rickerby, A. Matthews, A. Leyland, A. Pace and J. Valli, "The use of scratch adhesion testing for the determination of interfacial adhesion: the importance of frictional drag," *Surface and Coatings technology*, vol. 36, no. 1-2, pp. 503-517.
- [23] R.V. Williams, "Control and analysis in iron and steelmaking," 2016.
- [24] T.A. Taylor, *Thermal barrier coating for substrates and process for producing it*.
- [25] S. Bull and D. Rickerby, "New developments in the modelling of the hardness and scratch adhesion of thin films," *Surface and Coatings technology*, vol. 42, no. 2, pp. 149-164.